

# Capillarization of the Sinusoids in Liver Fibrosis: Noninvasive Assessment With Contrast-Enhanced MRI in the Rabbit

Bernard E. Van Beers,<sup>1\*</sup> Roland Materne,<sup>1</sup> Laurence Annet,<sup>1</sup> Laurent Hermoye,<sup>1</sup> Christine Sempoux,<sup>2</sup> Frank Peeters,<sup>1</sup> Anne M. Smith,<sup>1</sup> Jacques Jamart,<sup>3</sup> and Yves Horsmans<sup>4</sup>

**Sinusoidal capillarization induces microcirculatory changes in liver cirrhosis and fibrosis. The purpose of this study was to assess whether contrast-enhanced MRI can be used to demonstrate the effects of sinusoidal capillarization in liver fibrosis. Dynamic MRI after injection of a low-molecular-weight contrast agent of 0.56 kDa (Gd-DOTA), and two high-molecular-weight contrast agents of 6.47 kDa and 52 kDa (P792 and P717) was performed in rabbits with liver fibrosis induced by cholesterol and diethylstilbestrol. The hepatic distribution volume accessible to the high-molecular-weight agents decreased in the rabbits with liver fibrosis (P792:  $7.8\% \pm 1.7\%$  vs.  $10.1\% \pm 1.8\%$  in normal rabbits,  $P = .038$ ; P717:  $6.2\% \pm 2.1\%$  vs.  $9.7\% \pm 1.6\%$  in normal rabbits,  $P = .007$ ), whereas the hepatic mean transit time (MTT) of the low-molecular-weight agent was increased ( $15.9 \pm 8.0$  s vs.  $8.8 \pm 2.6$  s in normal rabbits,  $P = .015$ ). In rabbits with liver fibrosis, the clearance of indocyanine green (ICG) was correlated with the volume accessible to the high-molecular-weight agents (P792:  $r = 0.810$ ,  $P = .015$ ; P717:  $r = 0.857$ ,  $P = .007$ ). The collagen content of the liver was inversely correlated with the distribution volume of P717 ( $r = -.833$ ,  $P = .010$ ) and with the ICG clearance ( $r = -.810$ ,  $P = .015$ ). It was concluded that the microcirculatory changes induced by sinusoidal capillarization in liver fibrosis can be demonstrated noninvasively with MRI. Magn Reson Med 49:692–699, 2003. © 2003 Wiley-Liss, Inc.**

**Key words:** liver cirrhosis; physiopathology; liver blood supply; contrast media

The clearance of endo- and xenobiotics, which is one of the main functions of the liver, is markedly altered in cirrhosis and fibrosis (1). Two major factors that may affect the metabolism of drugs and endogenous substances in liver disease are the decrease of intrinsic hepatocellular clearance and the occurrence of vascular abnormalities.

These vascular abnormalities include the development of intra- and extrahepatic vascular shunts and the capillarization of liver sinusoids (2–5). Sinusoidal capillarization consists of transformation of the fenestrated hepatic sinusoids into continuous capillaries, with collagenization of the extravascular spaces of Disse and deposition of basement membranes near the endothelial cells and the hepatocytes (6). The microcirculatory changes induced by sinusoidal capillarization have been evaluated in previous studies with the multiple indicator dilution technique (3,7–9). This invasive method requires simultaneous catheterization of the portal vein (or the hepatic artery) and the hepatic vein to inject radiolabeled substances of different molecular weights. Because of its invasiveness, this method has limited clinical application and has mainly been used *ex vivo* (3,8,9).

MRI following intravenous injection of extracellular contrast agents has recently been described and validated to assess perfusion parameters in the liver (10). With this method, arterial and portal inflow, distribution volume, and mean transit time (MTT) of the contrast agents can be measured noninvasively. The purpose of the present study was to assess whether contrast-enhanced MRI using low- and high-molecular-weight contrast agents can be used to demonstrate the effects of sinusoidal capillarization in liver fibrosis induced by cholesterol and diethylstilbestrol in the rabbit.

## MATERIALS AND METHODS

### Animal Model

Experiments were performed on 16 male New Zealand White rabbits (Iffa Credo, Brussels, Belgium). The study protocol was approved by the Ethics Committee on Animal Care of our institution. The animals were housed in individual cages at 19°C with a 12-hr light/dark schedule, and fed rabbit chow and water *ad libitum*. The experimental group consisted of eight rabbits in which hepatic sinusoidal fibrosis was induced with a supplement of 2% cholesterol mixed in standard rabbit chow (ICN Biomedicals, Asse, Belgium) and subcutaneous administration of diethylstilbestrol (10 mg dissolved in 0.5 mL of corn oil twice weekly) for 12 weeks (11). The control group consisted of eight rabbits that received no treatment.

### Morphological Studies

At the end of the 12-week treatment, a median laparotomy was performed in the rabbits of the experimental group,

<sup>1</sup>Department of Radiology, Université Catholique de Louvain, St-Luc University Hospital, Brussels, Belgium.

<sup>2</sup>Department of Pathology, Université Catholique de Louvain, St-Luc University Hospital, Brussels, Belgium.

<sup>3</sup>Center of Biostatistics and Medical Documentation, Université Catholique de Louvain, Mont-Godinne University Hospital, Yvoir, Belgium.

<sup>4</sup>Laboratory of Gastroenterology, Université Catholique de Louvain, St-Luc University Hospital, Brussels, Belgium.

Grant sponsor: Fonds National de la Recherche Scientifique, Belgium; Grant number: FRSM 3.4578.00.

\*Correspondence to: Bernard E. Van Beers, M.D., Ph.D., Department of Radiology, Université Catholique de Louvain, St-Luc University Hospital, Avenue Hippocrate 10, B-1200 Brussels, Belgium.  
E-mail: vanbeers@rdgn.ucl.ac.be

Received 21 May 2002; revised 25 November 2002; accepted 26 November 2002.

DOI 10.1002/mrm.10420

Published online in Wiley InterScience (www.interscience.wiley.com).

© 2003 Wiley-Liss, Inc.

and surgical biopsies (diameter: 7–8 mm) were taken in the right liver lobe. Liver biopsies were also obtained in two rabbits of the control group. Liver slices were fixed in Bouin's solution for 24 hr and embedded in paraffin. General histological features were assessed on hematoxylin-eosin-stained sections and fibrosis was evaluated with Sirius red and Masson's Trichrome staining. Liver fibrosis was estimated by measuring the collagen content as previously described (12). Briefly, Masson's Trichrome-stained liver sections were digitized through a Leitz Ortholux microscope (Wetzlar, Germany) coupled with a JVC KY-F58 color digital camera (Victor Company of Japan, Yokohama, Japan). Fibrotic areas (blue-stained) and total sample areas were measured by a KS-400 system (Zeiss-Vision, Munich, Germany) and their ratios were expressed as percentages.

Small pieces of the liver were also taken from all rabbits in the experimental group for transmission electron microscopy (TEM). These specimens were fixed by immersion in cold 2.5% glutaraldehyde solution and postfixed in 1% osmium tetroxide before they were embedded in Epon (Fluka Chemie, Buchs, Switzerland). Ultrathin sections were counterstained with uranyl acetate and lead citrate, and examined with an EM 109 Zeiss (Oberkochen, Germany) electron microscope.

### Biochemical Tests

Venous blood samples were obtained in the experimental group before the start and at the end of the 12-week treatment. Biochemical analyses were performed on heparinized plasma with a standard clinical automated analyzer. Indocyanine green (ICG) clearance was measured in the experimental and control groups as previously described (13).

### MRI

The rabbits were anesthetized by intramuscular injection of ketamine hydrochloride (35 mg/kg) and xylazine hydrochloride (8 mg/kg) after an 18-hr fast. Additional doses of ketamine (17 mg/kg) and xylazine (4 mg/kg) were given about 1, 2, and 3 hr after the start of the anesthesia. The timing for these additional doses was based on the presence of palpebral and ear-pinch reflexes. The MR studies were performed 30 min after the start of the anesthesia because it is known that xylazine causes a drop in arterial pressure that predominates during the first minutes after induction. The studies were done on a 1.5 T scanner (Gyrosan NT Intera T15; Philips Medical Systems, Best, The Netherlands) with a fast T1-weighted spoiled gradient-echo sequence preceded by a non-slice-selective 90° preparation pulse and a spoiler gradient (10). A single slice level, which included the right liver lobe, aorta, and portal vein, was continuously scanned after contrast material injection with the following parameters: image thickness = 4 mm, TR/TE = 6.8/2 ms, flip angle = 45°, two signal acquisitions, field of view (FOV) = 20 cm with 60% rectangular FOV, matrix = 256 × 128, linear phase-encoding order, effective preparation time = 290 ms, and acquisition time per image = 1.1 s (Fig. 1). As a result, 120 images were recorded in 132 s. The contrast material

was manually injected at the beginning of the MR data acquisition through a 24-gauge catheter placed in the central ear vein, and flushed by 5 mL of saline solution. All bolus injections were performed by one investigator.

The contrast agents used in this study were a commercially-available, low-molecular-weight gadolinium chelate (Gd-DOTA [gadoterate dimeglumine, Dotarem®; Guerbet, Roissy, France]), and two experimental high-molecular-weight agents (P792 and P717; Guerbet). P792 is a macromolecular derivative of Gd-DOTA, and P717 is a dextran-Gd-DOTA derivative (14–16). The molecular weights of Gd-DOTA, P792, and P717 are 0.56, 6.47, and 52 kDa, respectively. According to these differences in molecular weight and size, differences in plasma clearance and distribution volume are observed between the three contrast agents (Table 1) (16). The contrast agents remain extracellular and are excreted by renal glomerular filtration. Gd-DOTA and P792 are excreted freely, whereas the urinary excretion of P717 is more restricted (14). The MR studies were performed first with Gd-DOTA (0.05 mmol kg<sup>-1</sup>) and were repeated with P792 (0.005 mmol kg<sup>-1</sup>) and P717 (0.017 mmol kg<sup>-1</sup>) with a time interval of at least 60 min between each examination. A lower dose was used for the high-molecular-weight agents because of their higher relaxivity (Table 1). The order of injection of the contrast agents was the same in all rabbits to allow for renal excretion of the low-molecular-weight agent, before the injection of the agents with higher molecular weight. The absence of any significant hemodynamic effect from the intravenous injection of these contrast agents has been reported previously in the rat (16,17).

At the end of the experiments, the animals were killed by intravenous administration of pentobarbital. The liver and spleen were dissected and weighed. Because only a single slice was imaged with MR, no attempt was made to grade the fibrosis in the whole liver.

### Image Analysis

Data processing was performed on a Silicon Graphics O2 workstation (Silicon Graphics Inc., Mountain View, CA), using programs written in IDL (Research Systems Inc., Boulder, CO), as previously described (18). Briefly, signal intensity vs. time curves were obtained by manually drawing regions of interest (ROIs) in the aorta, portal vein, and liver. The surface of the ROIs was at least 10 mm<sup>2</sup> in the vessels and 100 mm<sup>2</sup> in the liver. The first time points of the signal intensity vs. time curves were averaged and subtracted from the subsequent time points to ensure that the initial signal intensity was zero. The signal intensity vs. time curves were converted into longitudinal relaxation rate ( $R_1$ ) vs. time curves according to an in vitro calibration curve (10,19). A scaling factor was used to correct for differences in signal reception between the in vivo and the in vitro studies. The scaling factor was determined by dividing the signal intensity of a tube containing copper sulfate and agar in the in vivo studies by its signal intensity in the in vitro calibration study (10). Next, a linear relationship was assumed between  $R_1$  and contrast agent concentration, according to the equation:

$$R_1 = R_{1,post} - R_{1,pre} = r_1 C, \quad [1]$$

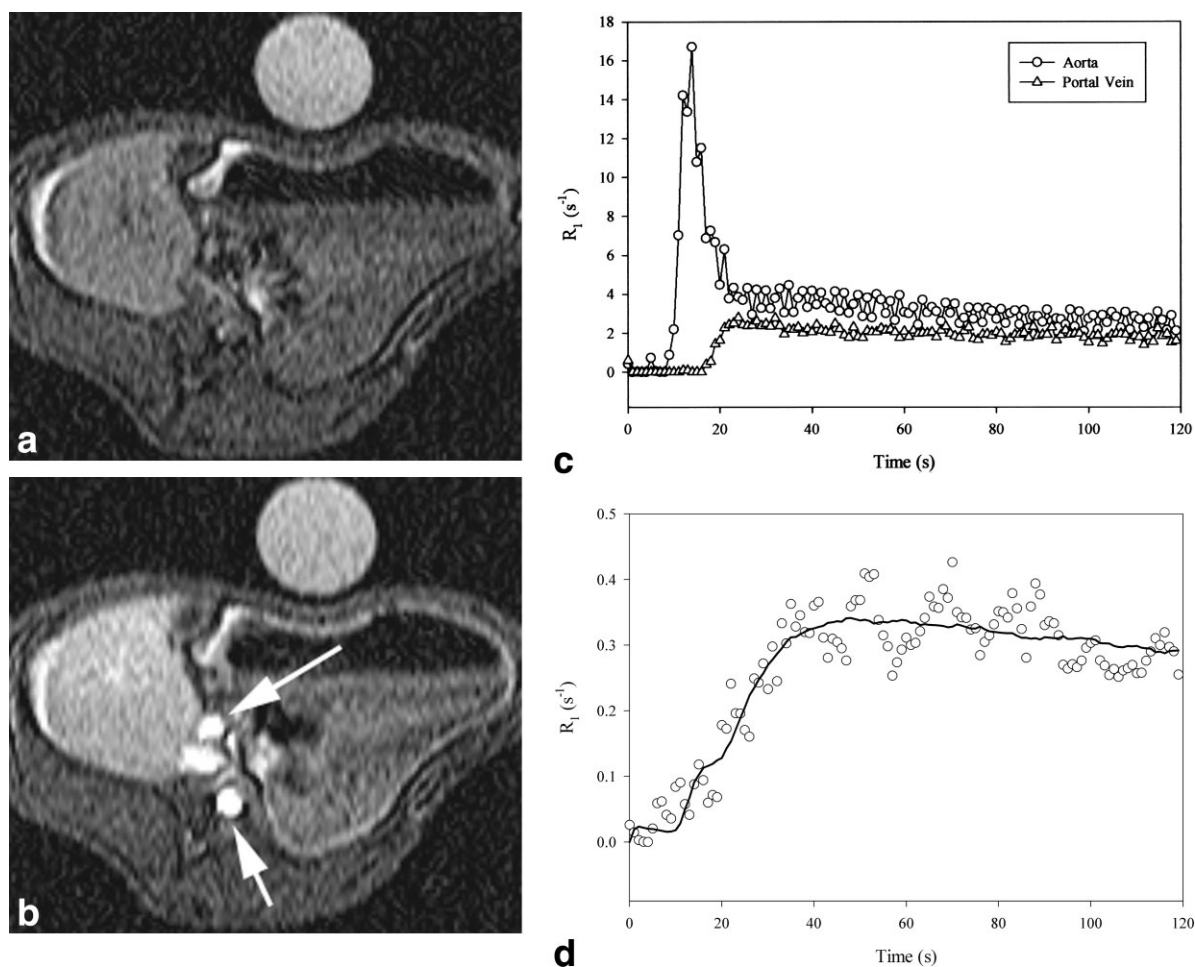


FIG. 1. Representative MR images (a) before and (b) after injection of  $0.05 \text{ mmol kg}^{-1}$  Gd-DOTA, and the corresponding relaxation rate vs. time curves in (c) the aorta and portal vein and (d) the liver. The long arrow in b indicates the portal vein, and the short arrow indicates the aorta. Dots in d represent the measured data, and the solid line is the reconstructed curve based on the estimated parameters ( $k_{1a} = 9.52 \text{ mL min}^{-1} 100 \text{ mL}^{-1}$ ,  $k_{1p} = 51.36 \text{ mL min}^{-1} 100 \text{ mL}^{-1}$ ,  $k_2 = 0.077 \text{ s}^{-1}$ ,  $\tau_a = \tau_p = 2 \text{ s}$ ).

where  $R_{1post}$  is the postcontrast longitudinal relaxation rate,  $R_{1pre}$  the precontrast longitudinal relaxation rate,  $r_1$  the longitudinal relaxivity of the contrast agent, and  $C$  its concentration. In this equation, it is assumed that the relaxivity of the contrast agent remains constant in blood and liver, and that the exchanges of water between intravascular, extravascular, and intracellular spaces are fast. These assumptions remain debated (20–22).

The time curves were analyzed with a dual-input one-compartmental model, on the basis of the equation:

$$\frac{dC_L(t)}{dt} = k_{1a}C_a(t) + k_{1p}C_p(t) - k_2C_L(t), \quad [2]$$

where  $C_a$  and  $C_p$  ( $\text{g mL}^{-1}_{\text{plasma}}$ ) are the concentrations of the contrast agents in the plasma of the hepatic artery and the portal vein;  $C_L$  ( $\text{g mL}^{-1}_{\text{liver}}$ ) is the concentration of the contrast agents in the liver;  $k_{1a}$  and  $k_{1p}$  ( $\text{mL}_{\text{plasma}} \text{ s}^{-1} \text{ mL}^{-1}_{\text{liver}}$ ) represent the aortic and portal venous plasma inflow, respectively; and  $k_2$  ( $\text{s}^{-1}$ ) represents the outflow rate. Two inputs are considered because the blood flows to the liver through both the hepatic artery and the portal vein. In this one-compartmental model, the tissue (here the liver) including the cells, extravascular space, and exchanging capillaries (sinusoids), is considered to be a single compartment, i.e., a region with an outflow concentration proportional to the concentration of the contrast agent inside

Table 1  
Physicochemical and Pharmacokinetic Parameters of Gd-DOTA, P792, and P717 in Rabbits

	Gd-DOTA	P792	P717
Molecular weight (kDa)	0.56	6.47	52
Longitudinal relaxivity ( $\text{L mmol}^{-1} \text{ s}^{-1}$ ) in water at 60 MHz and 37°C	2.9	29	9.4
Distribution volume ( $\text{mL kg}^{-1}$ )	187	101	<100
Plasma clearance ( $\text{mL min}^{-1} \text{ kg}^{-1}$ )	2.8	2.8	<2

it (10,19,23,24). The one-compartment model thus differs from the two-compartment model in which the liver is separated into two spaces (the sinusoids and extravascular space), as reported by Tofts et al. (25). In the Tofts model, the contribution of the intravascular tracer to the total tissue concentration is ignored. Ignoring the intravascular contribution of the tracer in the liver may introduce substantial errors, because the sinusoidal volume in the normal liver is larger than the extravascular extracellular space (8). With the one-compartmental model used in the present study, the sinusoidal contribution is taken into account in the liver compartment. In this model, the distribution volume includes the extravascular space and the sinusoids.

Solving for  $C_L(t)$ , we obtain:

$$C_L(t) = \int_0^t [k_{1a}C_a(t' - \tau_a) + k_{1p}C_p(t' - \tau_p)]e^{-k_2(t-t')} dt', \quad [3]$$

where  $t'$  is a dummy integration variable. Two delay parameters,  $\tau_a$  and  $\tau_p$ , were added in Eq. [3]. They represent the transit time from the aorta and portal vein regions to the liver ROI. The two delays were defined to be equal and were fixed to the delay between the first nonzero value of the  $C_a(t)$  curve and the first nonzero value of the  $C_L(t)$  curve. An unweighted least-squares fit using the Levenberg-Marquardt method (26) for the three parameters  $k_{1a}$ ,  $k_{1p}$ , and  $k_2$  of Eq. [3] was performed (Fig. 1).

The global inflow from plasma to the liver compartment ( $k_1$ ) was calculated as  $(k_{1a} + k_{1p})$ . To obtain the coefficients  $k_{1a}$  and  $k_{1p}$  expressed in  $(\text{mL min}^{-1} 100 \text{ mL}^{-1})$ , the coefficients expressed in  $(\text{mL}_{\text{plasma}} \text{ s}^{-1} \text{ mL}_{\text{liver}}^{-1})$  were multiplied by  $60 \text{ s min}^{-1}$  and by 100. Arterial and portal inflow fractions were obtained by dividing, respectively,  $k_{1a}$  and  $k_{1p}$  by  $k_1$ . The fractional distribution volume (%) of the contrast agent in the liver was calculated as  $100 k_1 k_2^{-1}$ . The MTT (s) was calculated as  $k_2^{-1}$ .

### Statistical Analysis

Numerical variables are expressed as mean  $\pm$  standard deviation (SD). Statistical analysis was performed with the SPSS software (SPSS Inc., Chicago, IL). Data were compared with the Wilcoxon signed-rank test when paired, and with the Wilcoxon rank-sum test when unpaired. Correlations were assessed with Spearman rank correlation coefficients. A  $P$ -value  $< .05$  was considered statistically significant.

## RESULTS

### Morphological Studies

The body weight of the rabbits was  $4.2 \pm 0.2 \text{ kg}$  in the control group and  $4.2 \pm 0.4 \text{ kg}$  in the experimental group. The liver weight was significantly higher in the experimental group than in the control group ( $159.8 \pm 31.6 \text{ g}$  vs.  $92.8 \pm 12.8 \text{ g}$ ,  $P < .001$ ), as was the spleen weight ( $4.1 \pm 1.2 \text{ g}$  vs.  $1.1 \pm 0.4 \text{ g}$ ,  $P < .001$ ).

In the two rabbits of the control group in which a biopsy was performed, liver histology was normal. In the eight

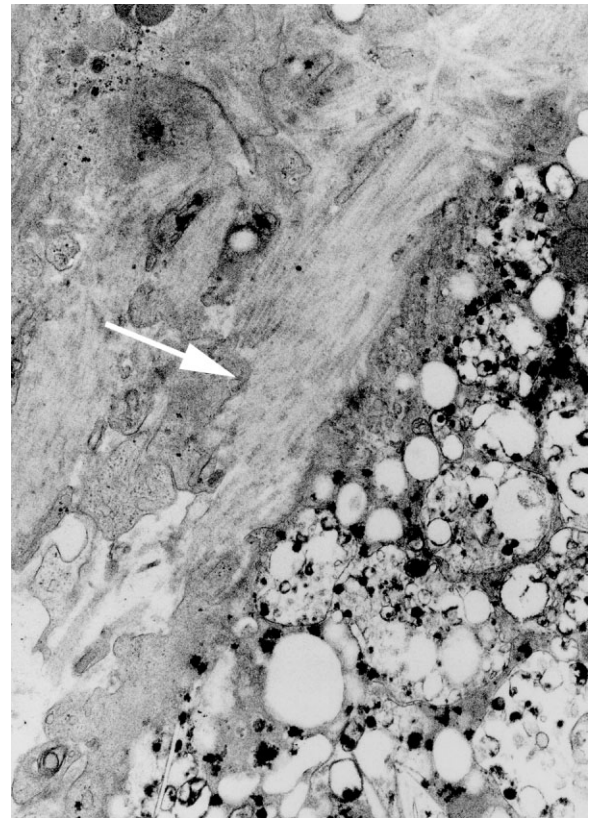


FIG. 2. Transmission electron micrograph ( $\times 20,200$ ) of the liver of a rabbit in the experimental group. Heavy deposition of collagen fibers (arrow) in the space of Disse is observed. Note the presence of numerous lipid droplets and phagolysosomes with debris in the cytoplasm of adjacent hepatocytes.

rabbits of the experimental group, the liver parenchyma was characterized by the development of moderate to severe irregular fibrosis located around the central veins and in adjacent sinusoids. In advanced lesions, there was a heavy deposition of collagen in the pericentral sinusoidal lumens, which sometimes replaced the hepatic plates with thin septa between central veins and portal tracts. The hepatocytes were enlarged because they contained numerous small lipid droplets in their cytoplasm. The collagen content of the liver was  $12\% \pm 8\%$  in the eight rabbits of the experimental group, whereas it was  $< 3\%$  in the two normal rabbits.

At electron microscopy, numerous collagen fibers were observed in the space of Disse (Fig. 2), as well as basement membranes adjacent to endothelial cells and hepatocytes (Fig. 3). Fat droplets and phagolysosomes containing myelin figures were seen in the cytoplasm of the liver cells.

### Biochemical Tests

The biochemical measurements obtained in the experimental group before and after the 12-week treatment are given in Table 2. The rabbits with liver fibrosis developed hemolytic anemia at the end of the treatment, with a significant decrease of their erythrocyte count, hemoglobin, and hematocrit ( $P = .012$ ). The number of platelets was significantly increased in the experimental group ( $P =$

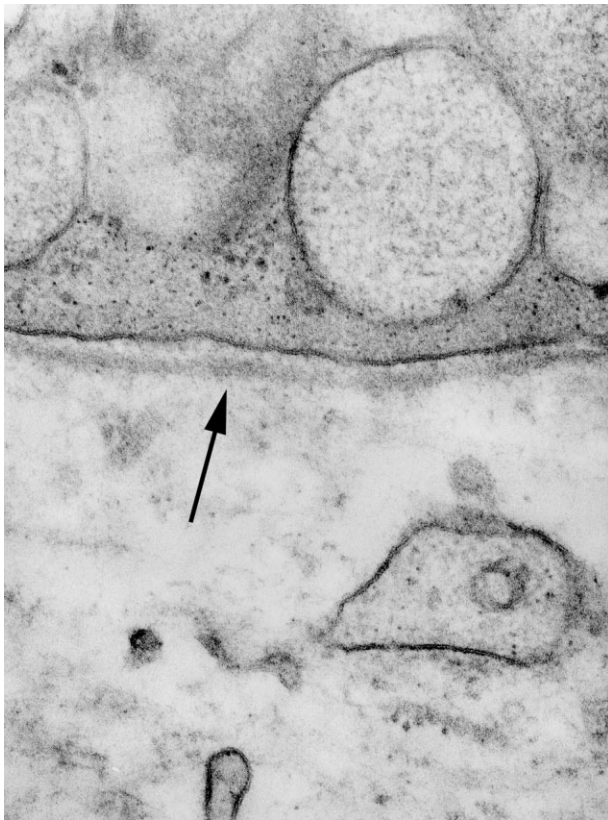


FIG. 3. Transmission electron micrograph ( $\times 159,000$ ) of the liver of a rabbit in the experimental group. Basement membrane (arrow) is seen between the hepatocyte and the endothelial cell.

.025), while the liver function tests showed a significant increase in lactate dehydrogenase and aminotransferases levels ( $P = .012$ ).

Hepatic sinusoidal fibrosis significantly decreased the clearance of ICG. Its plasma clearance was  $39.6 \pm 14.6 \text{ mL min}^{-1} \text{ kg}^{-1}$  in the control group, and  $14.6 \pm 5.5 \text{ mL min}^{-1} \text{ kg}^{-1}$  in the experimental group ( $P < .001$ ).

### MRI

There were no adverse reactions after the injection of the contrast agents in any of the 48 MR studies. The global hepatic inflow obtained with each contrast agent in the control and experimental groups is shown in Fig. 4a. The

Table 2  
Biochemical Data Obtained in Eight Rabbits With Liver Fibrosis\*

	Basal	12 Weeks
Hemoglobin ( $\text{g dL}^{-1}$ )	$13.8 \pm 1.1$	$7.5 \pm 1.8^a$
Hematocrit (%)	$41.8 \pm 3.4$	$22.4 \pm 4.8^a$
Erythrocyte count ( $10^{12} \text{ L}^{-1}$ )	$6.57 \pm 0.87$	$3.27 \pm 0.95^a$
Platelets ( $10^9 \text{ L}^{-1}$ )	$296 \pm 67$	$492 \pm 155^a$
Aspartate aminotransferase ( $\text{IU L}^{-1}$ )	$48 \pm 33$	$90 \pm 52^a$
Alanine aminotransferase ( $\text{IU L}^{-1}$ )	$68 \pm 30$	$102 \pm 43^a$
Lactate dehydrogenase ( $\text{IU L}^{-1}$ )	$138 \pm 44$	$233 \pm 77^a$

\*Data are expressed as mean  $\pm$  SD.

<sup>a</sup> $P < .05$  when compared with basal data.

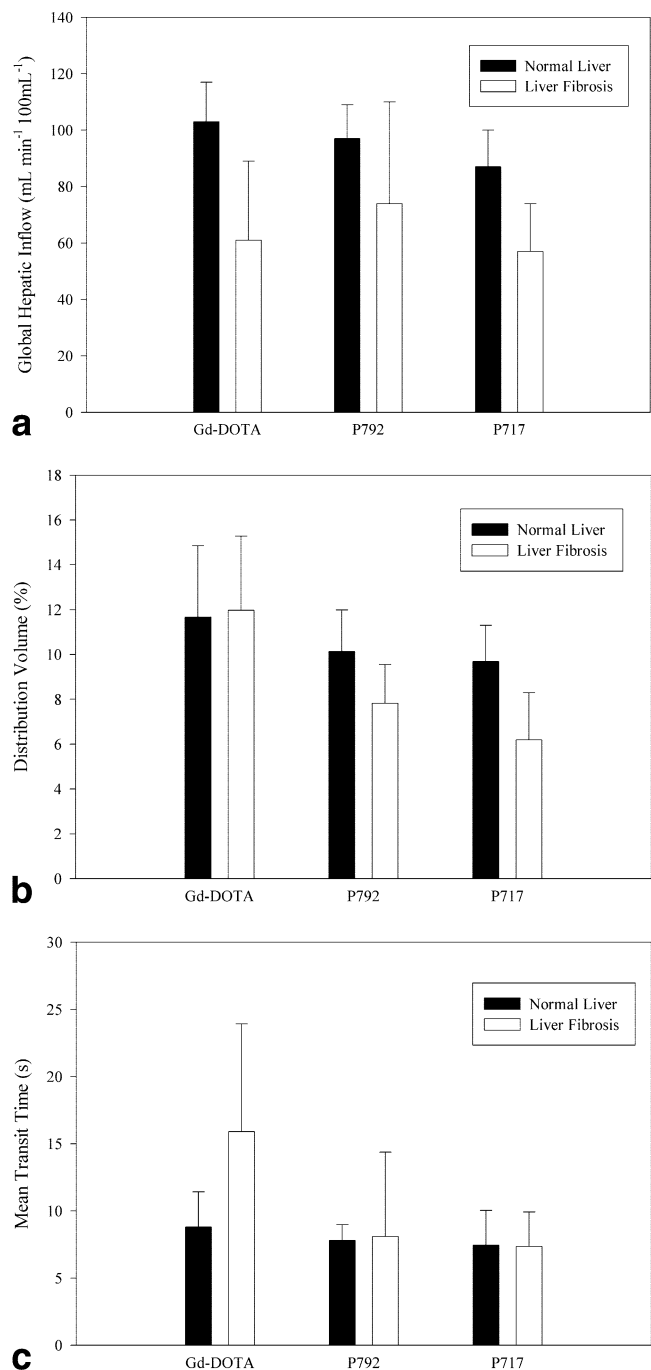


FIG. 4. Bar graphs of (a) global hepatic inflow, (b) distribution volume, and (c) MTT of low-molecular-weight agent Gd-DOTA and high-molecular-weight agents P792 and P717 in eight normal rabbits and eight rabbits with liver fibrosis. **a:** Hepatic inflow is significantly decreased in rabbits with liver fibrosis relative to normal rabbits when the low-molecular-weight agent Gd-DOTA ( $P = .007$ ) and the high-molecular-weight agent P717 ( $P = .005$ ) are used. Error bars represent the SD. **b:** Distribution volumes accessible to high-molecular-weight agents are significantly decreased in rabbits with liver fibrosis (P792:  $P = .038$ , P717:  $P = .007$ ). **c:** The MTT of the low-molecular-weight agent is significantly increased ( $P = .015$ ).

global inflow was lower in the rabbits with liver fibrosis than in the normal animals. A significant difference was observed with Gd-DOTA ( $61 \pm 28 \text{ mL min}^{-1} 100 \text{ mL}^{-1}$  in liver fibrosis vs.  $103 \pm 14 \text{ mL min}^{-1} 100 \text{ mL}^{-1}$  in normal livers,  $P = .007$ ) and with P717 ( $57 \pm 17 \text{ mL min}^{-1} 100 \text{ mL}^{-1}$  in liver fibrosis vs.  $87 \pm 13 \text{ mL min}^{-1} 100 \text{ mL}^{-1}$  in normal livers,  $P = .005$ ), while the decrease was not significant with P792 ( $74 \pm 36 \text{ mL min}^{-1} 100 \text{ mL}^{-1}$  vs.  $97 \pm 12 \text{ mL min}^{-1} 100 \text{ mL}^{-1}$ ). Similarly, the portal inflow was decreased in rabbits with liver fibrosis. Again, a significant difference of portal inflow was observed with Gd-DOTA ( $41 \pm 24 \text{ mL min}^{-1} 100 \text{ mL}^{-1}$  in liver fibrosis vs.  $86 \pm 11 \text{ mL min}^{-1} 100 \text{ mL}^{-1}$  in normal livers,  $P < .001$ ) and with P717 ( $45 \pm 23 \text{ mL min}^{-1} 100 \text{ mL}^{-1}$  in liver fibrosis vs.  $71 \pm 10 \text{ mL min}^{-1} 100 \text{ mL}^{-1}$  in normal livers,  $P = .007$ ), but not with P792 ( $60 \pm 31 \text{ mL min}^{-1} 100 \text{ mL}^{-1}$  vs.  $80 \pm 12 \text{ mL min}^{-1} 100 \text{ mL}^{-1}$ ). In the control group, arterial fractions were  $16\% \pm 5\%$  with Gd-DOTA,  $17\% \pm 5\%$  with P792, and  $18\% \pm 4\%$  with P717. In the experimental group, they were  $26\% \pm 33\%$ ,  $21\% \pm 11\%$ , and  $25\% \pm 31\%$ , respectively.

The distribution volume accessible to the high-molecular-weight contrast agents significantly decreased in rabbits with liver fibrosis (P792:  $7.8\% \pm 1.7\%$  vs.  $10.1\% \pm 1.8\%$  in normal rabbits,  $P = .038$ ; P717:  $6.2\% \pm 2.1\%$  vs.  $9.7\% \pm 1.6\%$  in normal rabbits,  $P = .007$ ). No significant difference of distribution volume was found between the two groups with the low-molecular-weight agent ( $11.7\% \pm 3.1\%$  vs.  $12.0\% \pm 3.3\%$ ) (Fig. 4b).

A significant increase in the MTT of the low-molecular-weight agent was observed in the rabbits with liver fibrosis ( $15.9 \pm 8.0 \text{ s}$  vs.  $8.8 \pm 2.6 \text{ s}$  in normal rabbits,  $P = .015$ ), whereas the MTT obtained after injection of the high-molecular-weight agents did not differ between normal rabbits and rabbits with liver fibrosis (P792:  $8.1 \pm 6.3 \text{ s}$  vs.  $7.8 \pm 1.2 \text{ s}$  in normal rabbits, P717:  $7.3 \pm 2.6 \text{ s}$  vs.  $7.5 \pm 2.6 \text{ s}$  in normal rabbits) (Fig. 4c).

In rabbits with liver fibrosis, the ICG clearance was significantly correlated with the distribution volume of the

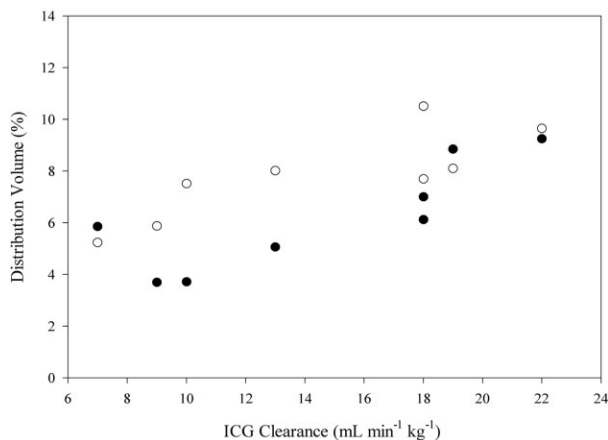


FIG. 5. Graphic representation of the correlation between the ICG clearance and distribution volume of high-molecular-weight agents. Significant correlations are observed between the ICG clearance and distribution volume of P792 ( $r = .810$ ,  $P = .015$ , white dots) and between the ICG clearance and distribution volume of P717 ( $r = .857$ ,  $P = .007$ , black dots).

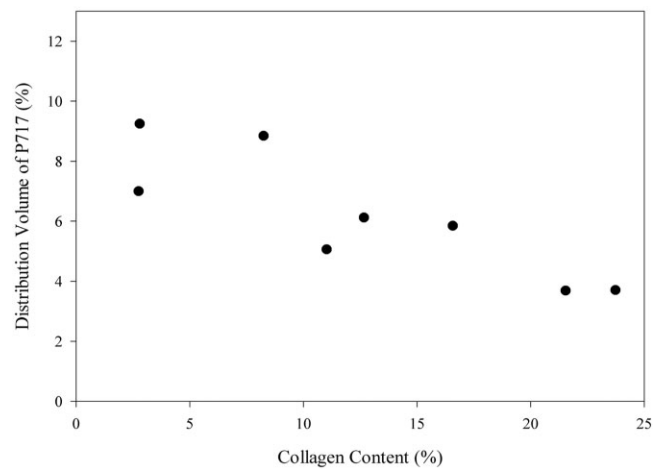


FIG. 6. Graphic representation of the correlation between the collagen content of the liver and the distribution volume of the high-molecular-weight agent P717 in rabbits with hepatic fibrosis. A significant inverse correlation is observed between the collagen content and distribution volume of P717 ( $r = -.833$ ,  $P = .010$ ).

high-molecular-weight agents (P792:  $r = .810$ ,  $P = .015$ ; P717:  $r = .857$ ,  $P = .007$ ) (Fig. 5), but not with that of the low-molecular-weight agent ( $r = .143$ ). The collagen content of the liver was significantly correlated with the distribution volume of P717 ( $r = -.833$ ,  $P = .010$ ) (Fig. 6), but not with the distribution volume of P792 ( $r = -.524$ ) or Gd-DOTA ( $r = -.167$ ). In addition, the collagen content was significantly correlated with the ICG clearance ( $r = -.810$ ,  $P = .015$ ).

## DISCUSSION

The results of this study show that the distribution volume of high-molecular-weight contrast agents is limited in a model of sinusoidal fibrosis, whereas the MTT of a low-molecular-weight agent is increased. These functional changes were in relation to the morphological changes observed at optical and electron microscopy. In the normal liver, high- and low-molecular-weight agents have free access to the extravascular space of Disse through the endothelial fenestrae. In this model of liver fibrosis, collagenization of the spaces of Disse and deposition of basement membranes were observed. It has been postulated that this sinusoidal capillarization creates a new barrier between the sinusoids and the hepatocytes, thereby impairing the leakage of high-molecular-weight agents such as P792 and P717 into the spaces of Disse and decreasing their distribution volume (7). Low-molecular-weight agents such as Gd-DOTA still have access to the extravascular spaces, but their MTT is increased, probably because the diffusion in the extravascular space is slowed down. This decreased diffusion in the extravascular space may be explained by the increase of proteoglycans and glycoproteins in liver fibrosis (27). These macromolecular constituents form a network that offers considerable resistance to transport (28). The in vivo results observed in the present study are in agreement with the ex vivo results observed

with multiple indicators in human cirrhosis and in tetrachloride-induced liver fibrosis in the rat (3,7–9).

We also observed a significant correlation between the collagen content of the liver and the distribution volume of P717. This is an additional indication that high-molecular-weight agents can be used as markers of sinusoidal capillarization. No correlation, however, was found between the extent of fibrosis and the distribution volume of P792 or Gd-DOTA. This might indicate that agents with higher molecular weight (>50 kDa) are better suited to detect vascular permeability changes in the liver. Nevertheless, these results should be interpreted with some caution, because of the limited study population and possible regional variations in liver perfusion and fibrosis.

In the present study, the clearance of ICG, a dye that binds to albumin, was correlated with the distribution volume of the high-molecular-weight contrast agents and with the collagen content of the liver. The significant correlation between ICG clearance and collagen content was previously observed in the same model of liver fibrosis (5). The clearance of ICG is considered to be mainly influenced by liver perfusion in normal circumstances, but the use of the clearance of ICG as a measure of liver perfusion is debated because its hepatic extraction is intermediate and becomes low in liver cirrhosis and fibrosis (29,30). This decrease of the extraction fraction may be secondary to many factors, including intrahepatic shunting, capillarization of the sinusoids, reduced permeability of the hepatocyte sinusoidal membrane, and decreased hepatocyte metabolism (31,32). The correlations we observed between ICG clearance and P717 distribution volume, and between ICG clearance and collagen content indicate that the decreased clearance of ICG is related to sinusoidal capillarization in the present model. These results suggest the importance of permeability changes in the clearance of drugs with albumin binding (1).

In addition, we observed that the global hepatic inflow and portal inflow decreased in the rabbits with liver fibrosis. Similar decreases have been previously observed in humans with liver cirrhosis (33), and can be explained by the increased resistance of the liver in fibrosis and cirrhosis.

Intrahepatic shunts can develop in human cirrhosis (2). The shunted part of hepatic perfusion is not isolated in the present model. The shunted part can be assessed by fitting the arterial ( $f_a$ ) and portal ( $f_p$ ) fractions of the liver ROI as additional parameters. However, it has been shown in normal rabbits that this five-parameter fit ( $k_{1a}$ ,  $k_{1p}$ ,  $k_2$ ,  $f_a$ ,  $f_p$ ) gave poor results when compared with radiolabeled microsphere measurements (18). It is not relevant to take intrahepatic shunting into account in rabbits with cholesterol-diethylstilbestrol-induced fibrosis, because neither small nor large intrahepatic shunts are a common feature in this model (2). Shunting in human cirrhosis will have the same effect on the perfusion parameters measured with low- and high-molecular-weight agents. It will reduce the MTT and the distribution volume of the administered substances (2).

Our results show that sinusoidal capillarization in liver fibrosis affects the extravascular distribution of low- and high-molecular-weight agents. According to our data, these microcirculatory changes can be assessed noninva-

sively with MRI. Many methods have been developed to assess the microvascular changes in liver fibrosis and cirrhosis (28). Most methods are invasive or have practical limitations. As already mentioned, the clearance of ICG and sorbitol depends on many factors, including perfusion, permeability, and cellular metabolism (31,32). We believe that tracers that remain extracellular, as used in the present study, are better suited to assess the microcirculatory changes of liver fibrosis and cirrhosis, because the confounding effects of intracellular uptake, transport, and metabolism are avoided.

The present method can also be used with computed tomography (CT) (34). With CT, the spatial resolution is often higher than with MRI, and a linear relationship is observed between signal enhancement and concentration of the contrast agent. However, higher doses of contrast agent are needed for CT, which increases the risk of adverse events, especially when high-molecular-weight agents with restricted excretion are used. In addition, high-radiation doses can be administered when the same slice level is repeatedly scanned to build the signal intensity-time curves.

Our study has several limitations. First, the entire liver was not examined at MRI and histology. Regional variations of fibrosis and perfusion could not be taken into account. However, the biopsies were taken in the hepatic lobe where the ROIs were placed at MRI. Because we used large ROIs in the liver, in-plane variations of perfusion were averaged. The assessment of liver perfusion on a pixel-by-pixel basis has been reported previously (35), but was not attempted in the present study.

Several factors may induce errors in the calculation of the concentration of the contrast agent from the signal-intensity measurements. These factors include inflow effects, rate of water exchange between plasma, extravascular space, and cells, and changes of the relaxivity of the contrast agents according to the macromolecular content of the tissue environment (20–22). Inflow effects can be minimized by cardiac gating (image acquisition during diastole) or can be corrected on the basis of flow measurements in the aorta and portal vein using phase-contrast methods (36). The effects of water exchange can be minimized by using a short-TR gradient-echo sequence and low doses of contrast agents, as in the present study (20).

The use of a single-compartment model to calculate liver inflow should also be discussed. This model is analogous to the well-stirred model used in pharmacokinetic studies (31). This model assumes instantaneous mixing of the contrast agent in the liver. In contrast, distributed models assume that axial concentration gradients are present in the liver (37). As stated by Brix et al. (38), the apparent perfusion calculated with the compartmental model is higher than the true perfusion.

Finally, the injection of the three contrast agents was always performed in the same order, according to their molecular weights and plasma clearance. We cannot exclude the possibility that the prolonged anesthesia influenced the data obtained with the high-molecular-weight agents, especially P717 (39). This should not modify the validity of our conclusions, because the comparisons were done between the results obtained with the same contrast

agents and time points in normal rabbits and rabbits with liver fibrosis.

The two high-molecular-weight MR contrast agents used are research products. It has been demonstrated that the acute toxicity of P792 and P717 in mice is very low (14,16). In addition, the safety of P792 in humans was established in a phase I clinical trial (40).

In conclusion, our findings show that the microcirculatory changes caused by sinusoidal capillarization in liver fibrosis can be demonstrated noninvasively with contrast-enhanced MRI.

## REFERENCES

- Keiding S. Drug administration to liver patients: aspects of liver pathophysiology. *Semin Liver Dis* 1995;15:268–282.
- Huet PM, Pomier-Layrargues G, Villeneuve JP, Varin F, Viallet A. Intrahepatic circulation in liver disease. *Semin Liver Dis* 1986;6:277–286.
- Reichen J, Egger B, Ohara N, Zeltner TB, Zysset T, Zimmermann A. Determinants of hepatic function in liver cirrhosis in the rat. Multivariate analysis. *J Clin Invest* 1988;82:2069–2076.
- Morgan DJ, McLean AJ. Clinical pharmacokinetic and pharmacodynamic considerations in patients with liver disease. An update. *Clin Pharmacokinet* 1995;29:370–391.
- Mastai R, Laganier S, Wanless IR, Giroux L, Rocheleau B, Huet PM. Hepatic sinusoidal fibrosis induced by cholesterol and stilbestrol in the rabbit. II. Hemodynamic and drug disposition studies. *Hepatology* 1996;24:865–870.
- Schaffner F, Popper H. Capillarization of hepatic sinusoids in man. *Gastroenterology* 1963;44:239–242.
- Huet PM, Goresky CA, Villeneuve JP, Marleau D, Lough JO. Assessment of liver microcirculation in human cirrhosis. *J Clin Invest* 1982;70:1234–1244.
- Varin F, Huet PM. Hepatic microcirculation in the perfused cirrhotic rat liver. *J Clin Invest* 1985;76:1904–1912.
- Villeneuve JP, Dagenais M, Huet PM, Roy A, Lapointe R, Marleau D. The hepatic microcirculation in the isolated perfused human liver. *Hepatology* 1996;23:24–31.
- Materne R, Smith AM, Peeters F, Dehoux JP, Keyeux A, Horsmans Y, Van Beers BE. Assessment of hepatic perfusion parameters with dynamic MRI. *Magn Reson Med* 2002;47:135–142.
- Wanless IR, Belgiorio J, Huet PM. Hepatic sinusoidal fibrosis induced by cholesterol and stilbestrol in the rabbit. I. Morphology and inhibition of fibrogenesis by dipyrindamole. *Hepatology* 1996;24:855–864.
- Marbaix E, Kokorine I, Moulin P, Donneux J, Eeckhout Y, Courtoy PJ. Menstrual breakdown of human endometrium can be mimicked in vitro and is selectively and reversibly blocked by inhibitors of matrix metalloproteinases. *Proc Natl Acad Sci USA* 1996;93:9120–9125.
- Plevris JN, Jalan R, Bzeizi KI, Dollinger MM, Lee A, Garden OJ, Hayes PC. Indocyanine green clearance reflects reperfusion injury following liver transplantation and is an early predictor of graft function. *J Hepatol* 1999;30:142–148.
- Corot C, Schaefer M, Beate S, Bourrinet P, Zehf S, Benize V, Sabatou M, Meyer D. Physical, chemical and biological evaluations of CMD-A2-Gd-DOTA. A new paramagnetic dextran polymer. *Acta Radiol Suppl* 1997;412:91–99.
- Corot C, Violas X, Robert P, Port M. Pharmacokinetics of three gadolinium chelates with different molecular sizes shortly after intravenous injection in rabbits: relevance to MR angiography. *Invest Radiol* 2000;35:213–218.
- Port M, Corot C, Raynal I, Idee JM, Dencausse A, Lancelot E, Meyer D, Bonnemain B, Lautrou J. Physicochemical and biological evaluation of P792, a rapid-clearance blood-pool agent for magnetic resonance imaging. *Invest Radiol* 2001;36:445–454.
- Idee JM, Berthommier C, Goulas V, Corot C, Santus R, Hermine C, Schaefer M, Bonnemain B. Haemodynamic effects of macrocyclic and linear gadolinium chelates in rats: role of calcium and transmetallation. *Biometals* 1998;11:113–123.
- Materne R, Van Beers BE, Smith AM, Leconte I, Jamart J, Dehoux JP, Keyeux A, Horsmans Y. Non-invasive quantification of liver perfusion with dynamic computed tomography and a dual-input one-compartmental model. *Clin Sci* 2000;99:517–525.
- Vallee JP, Lazeyras F, Kasuboski L, Chatelain P, Howarth N, Righetti A, Didier D. Quantification of myocardial perfusion with FAST sequence and Gd bolus in patients with normal cardiac function. *J Magn Reson Imaging* 1999;9:197–203.
- Donahue KM, Weisskoff RM, Burstein D. Water diffusion and exchange as they influence contrast enhancement. *J Magn Reson Imaging* 1997;7:102–110.
- Landis CS, Li X, Telang FW, Coderre JA, Micca PL, Rooney WD, Latour LL, Vetek G, Palyka I, Springer CS. Determination of the MRI contrast concentration time course in vivo following bolus injection: effect of equilibrium transcytolemmal water exchange. *Magn Reson Med* 2000;44:563–574.
- Stanisz GJ, Henkelman RM. Gd-DTPA relaxivity depends on macromolecular content. *Magn Reson Med* 2000;44:665–667.
- Ziegler SI, Haberkorn U, Byrne H, Tong C, Schosser R, Krieter H, Kaja S, Richolt JA, Lammertsma AA, Price P. Measurement of liver blood flow using oxygen-15 labelled water and dynamic positron emission tomography: limitations of model description. *Eur J Nucl Med* 1996;23:169–177.
- Vallee JP, Sostman HD, MacFall JR, Wheeler T, Hedlund LW, Spritzer CE, Coleman RE. MRI quantitative myocardial perfusion with compartmental analysis: a rest and stress study. *Magn Reson Med* 1997;38:981–989.
- Tofts PS, Brix G, Buckley DL, Evelhoch JL, Henderson E, Knopp MV, Larsson HB, Lee TY, Mayr NA, Parker GJ, Port RE, Taylor J, Weisskoff RM. Estimating kinetic parameters from dynamic contrast-enhanced T<sub>1</sub>-weighted MRI of a diffusible tracer: standardized quantities and symbols. *J Magn Reson Imaging* 1999;10:223–232.
- Marquardt DW. An algorithm for least squares estimation of non-linear parameters. *J Soc Ind Appl Math* 1963;11:431–441.
- Murata K, Ochiai, Akashio K. Polydispersity of acidic glycosaminoglycan components in human liver and the changes at different stages in liver cirrhosis. *Gastroenterology* 1985;89:1248–1257.
- Nugent LJ, Jain RK. Extravascular diffusion in normal and neoplastic tissues. *Cancer Res* 1984;44:238–244.
- Molino G, Avagnina P, Belforte G, Bircher J. Assessment of the hepatic circulation in humans: new concepts based on evidence derived from a D-sorbitol clearance method. *J Lab Clin Med* 1998;131:393–405.
- Skak C, Keiding S. Methodological problems in the use of indocyanine green to estimate hepatic blood flow and ICG clearance in man. *Liver* 1987;7:155–162.
- Keiding S, Engsted E, Ott P. Sorbitol as a test substance for measurement of liver plasma flow in humans. *Hepatology* 1998;28:50–56.
- Ott P, Clemmesen O, Keiding S. Interpretation of simultaneous measurements of hepatic extraction fractions of indocyanine green and sorbitol: evidence of hepatic shunts and capillarization? *Dig Dis Sci* 2000;45:359–365.
- Van Beers BE, Leconte I, Materne R, Smith AM, Jamart J, Horsmans Y. Hepatic perfusion parameters in chronic liver disease: dynamic CT measurements correlated with disease severity. *Am J Roentgenol* 2001;176:667–673.
- Materne R, Annet L, Dechambre S, Sempoux C, Smith AM, Corot C, Horsmans Y, Van Beers BE. Dynamic computed tomography with low- and high-molecular-mass contrast agents to assess microvascular permeability modifications in a model of liver fibrosis. *Clin Sci* 2002;103:213–216.
- Leggett DA, Kelley BB, Bunce IH, Miles KA. Colorectal cancer: diagnostic potential of CT measurements of hepatic perfusion and implications for contrast enhancement protocols. *Radiology* 1997;205:716–720.
- Peeters F, Annet L, Hermoye L, Van Beers BE. Inflow effects in TFE-images with application to perfusion measurements. In: Proceedings of the 10th Annual Meeting of ISMRM, Honolulu, 2002. p 2303.
- Morgan DJ, Smallwood RA. Clinical significance of pharmacokinetic models of hepatic elimination. *Clin Pharmacokinet* 1990;18:61–76.
- Brix G, Bahner ML, Hoffmann U, Horvath A, Schreiber W. Regional blood flow, capillary permeability, and compartmental volumes: measurement with dynamic CT. Initial experience. *Radiology* 1999;210:269–276.
- Wyatt JD, Scott RA, Richardson ME. The effects of prolonged ketamine-xylozine intravenous infusion on arterial blood pH, blood gases, mean arterial blood pressure, heart and respiratory rates, rectal temperature and reflexes in the rabbit. *Lab Anim Sci* 1989;39:411–416.
- Gaillard S, Kubiak C, Stolz C, Bonnemain B, Chassard D. Safety and pharmacokinetics of P792, a new blood-pool agent: results of clinical testing in nonpatient volunteers. *Invest Radiol* 2002;37:161–166.